

# URG study of the Kondo model: unveiling the Kondo cloud

Anirban Mukherjee\* and Siddhartha Lal†

*Department of Physical Sciences, IISER Kolkata*

N.S. Vidhyadhiraja‡

*Theoretical Sciences Unit, JNCASR, Bangalore*

Arghya Tarapdher§

*Physics Department and Centre for Theoretical Studies, IIT Kharagpur*

(Dated: September 19, 2020)

# Abstract

To be written...

In this work, we will study the single channel Kondo problem via the URG approach, i.e., the physics of screening of a magnetic impurity via coupling with a conduction electron bath. The thermodynamic properties and universal characteristics of the single channel Kondo problem has been extensively studied in the past using various methods, starting from Kondo's perturbation theory solution [1], the Coulomb gas approach [2, 3], the poor man scaling approach [4], Bethe Ansatz calculations [5, 6], Wilson's numerical RG approach [7, 8] and the conformal field theory (CFT) approach [9, 10]. Another important strong coupling approach based on arguments of scattering phase shifts is that of the local Fermi liquid theory [11, 12].

However, the form of the effective Hamiltonian governing the low- energy physics of the Kondo cloud, and the form of the many-body singlet wavefunction, has remained a challenge. Further, the entanglement properties of the constituents of the Kondo cloud [13] is a matter of recent studies. The rest of the chapter is outlined as follows. In Sec.I, we introduce the single channel Kondo model, and perform a URG analysis of it in Sec.II. Sec.III constitutes results on the scaling of the Kondo coupling, various low-energy fixed points and their respective effective Hamiltonians and ground state wavefunction. In Sec.IV, we derive the local Fermi liquid theory. In Sec.V and Sec.VI, we compute various well studied thermodynamics signatures for the Kondo problem and benchmark them with the literature. In Sec.VII, we study the entanglement features and many-body correlations of the Kondo cloud. Finally, we conclude in Sec.VIII.

## I. THE MODEL

The Kondo model [1, 4] describes the coupling between a magnetic quantum impurity localized in real space with a bath of conduction electrons

$$\hat{H} = \sum_{\mathbf{k}\sigma} \epsilon_{\mathbf{k}} \hat{n}_{\mathbf{k}\sigma} + \frac{J}{2} \sum_{\mathbf{k}, \mathbf{k}'} \mathbf{S} \cdot c_{\mathbf{k}\alpha}^{\dagger} \boldsymbol{\sigma}_{\alpha\beta} c_{\mathbf{k}'\beta} . \quad (1)$$

---

\* am14rs016@iiserkol.ac.in

† slal@iiserkol.ac.in

‡ raja@jncasr.in

§ arghya@phy.kgp.ernet.in

Here, we consider a 2D electronic bath  $\epsilon_{\mathbf{k}} = -2t(\cos k_x + \cos k_y)$  with the Fermi energy  $E_F = \mu$ .  $J$  is the Kondo scattering coupling between the impurity and the conduction electrons. An important feature of the Kondo coupling is the two different classes of scattering processes: one involving spin-flip scattering processes for the bath electrons ( $c_{\mathbf{k}\uparrow}^\dagger c_{\mathbf{k}'\downarrow} + h.c.$ ), and the other not (i.e., simple potential scattering processes). In the antiferromagnetic regime  $J > 0$ , the spin-flip scattering processes generates quantum entanglement between the impurity spin and a macroscopic number of bath electrons (called the “Kondo cloud”), resulting in the complete screening of the impurity via the formation of a singlet spin state. It is clear that the dynamical Kondo cloud corresponds to an effective single spin-1/2, such that the screening is an example of macroscopic quantum entanglement arising from electronic correlations. It is the nature of this entanglement, and the underlying quantum liquid that forms the Kondo cloud, that we seek to learn more of.

## II. URG THEORY FOR THE KONDO MODEL

In constructing an effective low-energy theory for the Kondo singlet, we employ the unitary RG formalism to the Kondo model such that electronic states from the non-interacting conduction bath are stepwise disentangled, starting with the highest energy electrons at the bandwidth and eventually scaling towards the FS. While this aspect is similar to Anderson’s poor man’s scaling [4], we shall see that several other aspects of the unitary RG formalism are different from those adopted in the poor man’s scaling approach. The electronic states are labelled in terms of the normal distance  $\Lambda$  from the FS and the orientation unit vectors (Fig.2)  $\hat{s}$ :  $\mathbf{k}_{\Lambda\hat{s}} = \mathbf{k}_F(\hat{s}) + \Lambda\hat{s}$ , where  $\hat{s} = \frac{\nabla\epsilon_{\mathbf{k}}}{|\nabla\epsilon_{\mathbf{k}}|}|_{\epsilon_{\mathbf{k}}=E_F}$ . The states are labelled as  $|j, l, \sigma\rangle = |\mathbf{k}_{\Lambda_j\hat{s}}, \sigma\rangle$ ,  $l := (\hat{s}_m, \sigma)$ .

The  $\Lambda$ ’s are arranged as follows:  $\Lambda_N > \Lambda_{N-1} > \dots > 0$ , where the electronic states farthest from FS  $\Lambda_N$  are disentangled first, eventually scaling towards the FS. This leads to the Hamiltonian flow equation

$$H_{(j-1)} = U_{(j)} H_{(j)} U_{(j)}^\dagger, \quad (2)$$

where the unitary operation  $U_{(j)}$  is the unitary map at RG step  $j$ .  $U_{(j)}$  disentangles all the electronic states  $|\mathbf{k}_{\Lambda_j\hat{s}_m}, \sigma\rangle$  on the isogeometric curve and has the form[14]

$$U_{(j)} = \prod_l U_{j,l}, U_{j,l} = \frac{1}{\sqrt{2}}[1 + \eta_{j,l} - \eta_{j,l}^\dagger], \quad (3)$$

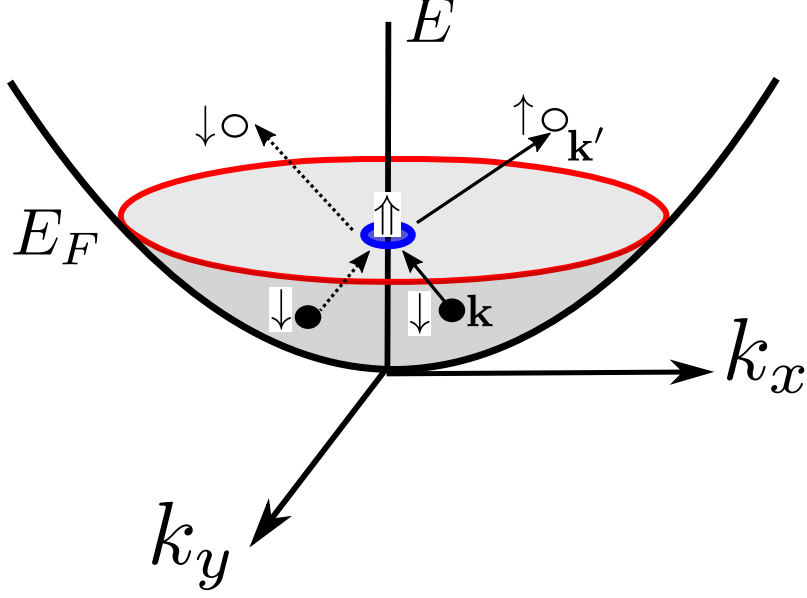


FIG. 1. The Kondo model is composed of a two-dimensional conduction electron bath (Fermi liquid) coupled to a magnetic impurity via a spin-flip (solid) / non spin-flip (dashed) scattering coupling.

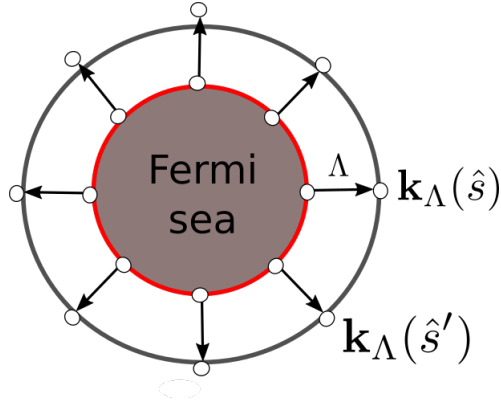


FIG. 2. Fermi surface geometry for a circular Fermi volume of non-interacting electrons in 2 spatial dimensions.

where  $\eta_{j,l}$  are electron-hole transition operators following the algebra

$$\{\eta_{j,l}, \eta_{j,l}^\dagger\} = 1, \quad [\eta_{j,l}, \eta_{j,l}^\dagger] = 1. \quad (4)$$

The transition operator can be represented in terms of the diagonal ( $H^D$ ) and off-diagonal ( $H^X$ ) parts of the Hamiltonian as follows

$$\eta_{j,l} = Tr_{j,l}(c_{j,l}^\dagger H_{j,l}) c_{j,l} \frac{1}{\hat{\omega}_{j,l} - Tr_{j,l}(H_{j,l}^D \hat{n}_{j,l}) \hat{n}_{j,l}}. \quad (5)$$

We note that in the numerator of the expression for  $\eta_{j,l}$ , the operator  $Tr_{j,l}(c_{j,l}^\dagger H_{j,l})c_{j,l} + h.c.$  is composed of all possible scattering vertices that modify the configuration of the electronic state  $|j, l\rangle$ . The generic forms of  $H_{j,l}^D$  and  $H_{j,l}^X$  are as follows

$$\begin{aligned} H_{j,l}^D &= \sum_{\Lambda \hat{s}, \sigma} \epsilon^{j,l} \hat{n}_{\mathbf{k}_{\Lambda \hat{s}, \sigma}} + \sum_{\alpha} \Gamma_{\alpha}^{4,(j,l)} \hat{n}_{\mathbf{k}\sigma} \hat{n}_{\mathbf{k}'\sigma'} + \sum_{\beta} \Gamma_{\beta}^{8,(j,l)} \hat{n}_{\mathbf{k}\sigma} \hat{n}_{\mathbf{k}'\sigma'} (1 - \hat{n}_{\mathbf{k}''\sigma''}) + \dots, \\ H_{j,l}^X &= \sum_{\alpha} \Gamma_{\alpha}^2 c_{\mathbf{k}\sigma}^\dagger c_{\mathbf{k}'\sigma'} + \sum_{\beta} \Gamma_{\beta}^2 c_{\mathbf{k}\sigma}^\dagger c_{\mathbf{k}'\sigma'} c_{\mathbf{k}_1'\sigma_1'} c_{\mathbf{k}_1\sigma_1} + \dots \end{aligned} \quad (6)$$

The operator  $\hat{\omega}_{j,l}$  accounts for the quantum fluctuations arising from the non-commutativity between different parts of the renormalized Hamiltonian and has the following form [15]

$$\hat{\omega}_{j,l} = H_{j,l}^D + H_{j,l}^X - H_{j,l-1}^X. \quad (7)$$

Upon disentangling electronic states  $\hat{s}, \sigma$  along a isogeometric curve at distance  $\Lambda_j$ , the following effective Hamiltonian  $H_{j,l}$  is generated

$$H_{j,l} = \prod_{m=1}^l U_{j,m} H_{(j)} \left[ \prod_{m=1}^l U_{j,m} \right]^\dagger. \quad (8)$$

We note that  $H_{j,2n_j+1} = H_{(j-1)}$  is the Hamiltonian obtained after disentangling all the electronic states on the isogeometric curve  $j$ . Below we depict the different terms generated upon successive disentanglement of the states  $|\mathbf{k}_{\Lambda_j \hat{s}_l}, \sigma\rangle$  on a given curve,

$$\begin{aligned} H_{j,l+1} &= Tr_{j,l}(H_{(j,l)}) + \{c_{j,l}^\dagger Tr_{j,l}(H_{(j,l)} c_{j,l}), \eta_{j,l}\} \tau_{j,l}, \tau_{j,l} = \hat{n}_{j,l} - \frac{1}{2} \\ H_{j,l+2} &= Tr_{j,l+1}(Tr_{j,l}(H_{(j,l)})) + Tr_{j,l+1}(\{c_{j,l}^\dagger Tr_{j,l}(H_{(j,l)} c_{j,l}), \eta_{j,l}\} \tau_{j,l}) \\ &\quad + \{c_{j,l+1}^\dagger Tr_{j,l+1}(Tr_{j,l}(H_{(j,l)} c_{j,l+1})), \eta_{j,l+1}\} \tau_{j,l+1} \\ &\quad + \{c_{j,l+1}^\dagger Tr_{j,l+1}(\{c_{j,l}^\dagger Tr_{j,l}(H_{(j,l)} c_{j,l}), \eta_{j,l}\} c_{j,l+1}), \eta_{j,l+1}\} \tau_{j,l} \tau_{j,l+1}. \\ H_{j,l+3} &= \dots \text{terms with } \tau_{j,l}, \tau_{j,l+1}, \tau_{j,l+2} \dots \\ &\quad + \dots \text{terms with } \tau_{j,l} \tau_{j,l+1}, \tau_{j,l+1} \tau_{j,l+2}, \tau_{j,l} \tau_{j,l+2} \dots \\ &\quad + \dots \text{terms with } \tau_{j,l} \tau_{j,l+1} \tau_{j,l+2}. \end{aligned} \quad (9)$$

Upon disentangling multiple electronic states placed in the tangential direction on a given momentum shell at distance  $\Lambda_j$  generates RG contribution from leading order scattering processes (terms multiplied with  $\tau_{j,l}$ ,  $\tau_{j,l+1}$ , etc.) that goes as  $Area/Vol = 1/L$  and higher order processes like terms multiplied with  $\tau_{j,l} \tau_{j,l+1}$  that goes as  $(Area)^2/Vol^2 = 1/L^2$ ,  $\tau_{j,l} \tau_{j,l+1} \tau_{j,l+2}$  that goes as  $(Area)^3/Vol^3 = 1/L^3$ . Here, each factor of area arises from

decoupling an entire shell of single-particle states  $(\tau_{j,l})$  at every RG step, and every factor of volume arises from the Kondo coupling. Accounting for only the leading tangential scattering processes, as well as other momentum transfer processes along the normal direction  $\hat{s}$ , the renormalized Hamiltonian has the form

$$H_{(j-1)} = Tr_{j,(1,\dots,2n_j)}(H_{(j)}) + \sum_{l=1}^{2n_j} \{c_{j,l}^\dagger Tr_{j,l}(H_{(j)}c_{j,l}), \eta_{j,l}\} \tau_{j,l}. \quad (10)$$

Here,  $2n_j$  are the number of electronic states on the isogeometric curve at distance  $\Lambda_j$ , and  $\tau_{j,l} = n_{j,l} - \frac{1}{2}$ .

From the effective Hamiltonian obtained at the stable fixed point  $\hat{H}^*$ , we can compute the (unnormalised) density matrix operator ( $\hat{\rho} = e^{-\beta\hat{H}^*}$ ) and thence the finite-temperature partition function as

$$\begin{aligned} Z &= \text{Tr} [\hat{\rho}] = \text{Tr} \left[ e^{-\beta\hat{H}^*} \right] \quad , \quad \beta = 1/k_B T \\ &= \text{Tr} \left[ U^\dagger e^{-\beta\hat{H}^*} U \right] \quad , \quad U = \prod_1^{j^*} U_{(j)} \\ &= \text{Tr} \left[ e^{-\beta\hat{H}} \right] \quad , \end{aligned} \quad (11)$$

where  $H$  is the bare Hamiltonian and  $j^*$  is the RG step at which the IR stable fixed point is reached. This indicates that the partition function is preserved along the RG flow as the unitary transformations preserve the eigenspectrum.

### III. RG FLOW TO THE IR FIXED POINT

The unitary RG process generates the effective Hamiltonian's  $\hat{H}_{(j)}(\omega)$ 's for various eigen directions  $|\Phi(\omega)\rangle$  of the  $\hat{\omega}$  operator. Note the associated eigenvalue  $\omega$  identifies a subspectrum in the interacting many body eigenspace. The form of  $\hat{H}_{(j)}(\omega)$  is given by,

$$\hat{H}_{(j)}(\omega) = \sum_{j,l,\sigma} \epsilon_{j,l} \hat{n}_{j,l} + \frac{J^{(j)}(\omega)}{2} \sum_{\substack{j_1, j_2 < j, \\ m, m'}} \mathbf{S} \cdot c_{j_1, \hat{s}_m, \alpha}^\dagger \boldsymbol{\sigma}_{\alpha\beta} c_{j_2, \hat{s}_{m'}, \beta} + \sum_{\substack{a=N, \\ m=1}}^{j, n_j} J^{(a)} S^z s_{a, \hat{s}, m}^z, \quad (12)$$

where  $s_{l, \hat{s}, m}^z = \frac{1}{2}(\hat{n}_{l, \hat{s}_m, \uparrow} - \hat{n}_{l, \hat{s}_m, \downarrow})$ . The Kondo coupling RG equation for the RG steps (Appendix VIII) has the form,

$$\frac{\Delta J^{(j)}(\omega)}{\Delta \log \frac{\Lambda_j}{\Lambda_0}} = \frac{n_j (J^{(j)})^2 \left[ \left( \omega - \frac{\hbar v_F \Lambda_j}{2} \right) \right]}{\left( \omega - \frac{\hbar v_F \Lambda_j}{2} \right)^2 - \frac{(J^{(j)})^2}{16}}, \quad (13)$$

where  $n_j = \sum_s 1$  is the number of states on the isogeometric shell at distance  $\Lambda_j$  from the Fermi surface. Note that the denominator  $\Delta \log \frac{\Lambda_j}{\Lambda_0} = 1$  for the RG scale parameterization  $\Lambda_j = \Lambda_0 \exp(-j)$ . We now redefine Kondo coupling as a dimensionless parameter

$$K^{(j)} = \frac{J^{(j)}}{\omega - \frac{\hbar v_F}{2} \Lambda_j}, \quad (14)$$

and operate in the regime  $\omega > \frac{\hbar v_F}{2} \Lambda_j$ . With the above parametrization of eq.(14), we can convert the difference RG relation (eq.(13)) into a continuum RG equation

$$\frac{dK}{d \log \frac{\Lambda}{\Lambda_0}} = \left(1 - \frac{\omega}{\omega - \hbar v_F \Lambda}\right) K + \frac{n(\Lambda) K^2}{1 - \frac{K^2}{16}} \quad (15)$$

Upon approaching the Fermi surface  $\Lambda_j \rightarrow 0$ ,  $\left(1 - \frac{\omega}{\omega - \hbar v_F \Lambda}\right) \rightarrow 0$  and  $n(\Lambda)$  can be replaced by density of states on the Fermi surface  $n(0)$ :

$$\frac{dK}{d \log \frac{\Lambda}{\Lambda_0}} = \frac{n(0) K^2}{1 - \frac{K^2}{16}} \quad (16)$$

At this point, we observe an important aspect of the RG equation: for  $K \ll 1$ , the

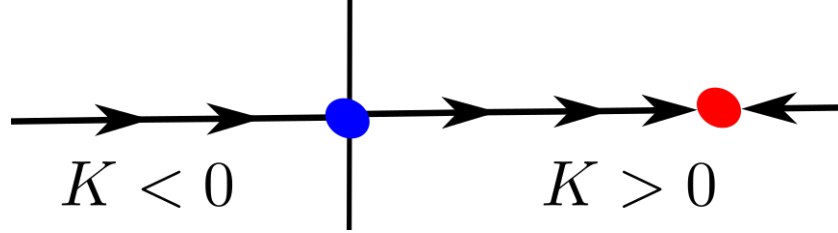


FIG. 3. Schematic RG phase diagram for the Kondo problem. The red dot represents intermediate coupling fixed point at  $K^* = 4$  for the case of the AFM Kondo coupling. The blue dot represents the critical fixed point at  $K^* = 0$  for the case of the FM Kondo coupling.

RG equation reduces to the one loop form:  $\frac{dK}{d \log \frac{\Lambda}{\Lambda_0}} = K^2$  [4]. On the other hand, the nonperturbative form of the flow equation obtained from the URG formalism shows the presence of intermediate coupling fixed point at  $K^* = 4$  in the antiferromagnetic regime  $K > 0$ . Upon integrating the RG equation and using the fixed point value  $K^* = 4$  we

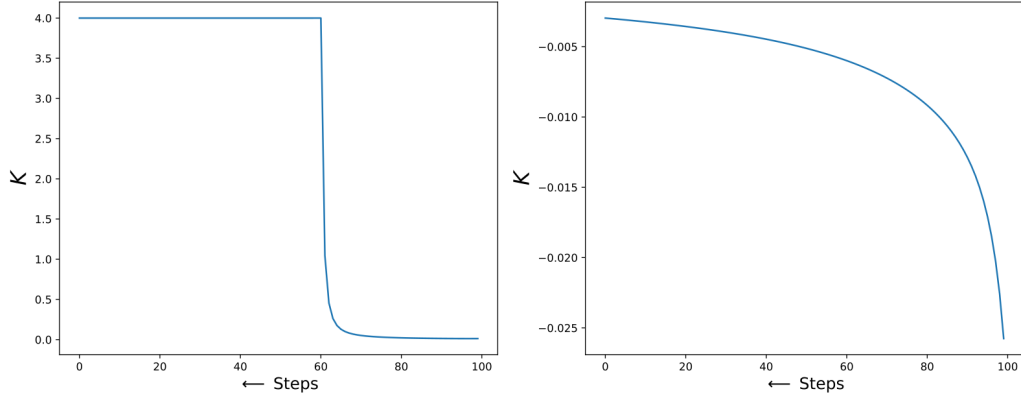


FIG. 4. Renormalized dimensionless Kondo coupling  $K$  with RG steps  $(\log \Lambda_j/\Lambda_0)$  for left panel:  $K > 0$ , and right panel:  $K < 0$ . The growth of the Kondo coupling to a finite value of the intermediate coupling fixed point is evident in the left panel, while the decay to zero at the critical fixed point can be seen in the right panel. For these plot, we chose  $\omega = \hbar v_F \Lambda_j$ .

obtain the Kondo energy scale ( $T_K$ ) and thence the effective length of the Kondo cloud ( $\xi_K$ )

$$\frac{1}{K_0} - \frac{1}{2} + \frac{K_0}{16} = -n(0) \log \frac{\Lambda^*}{\Lambda_0}, \quad (17)$$

$$\Lambda^* = \Lambda_0 \exp \left( \frac{1}{2n(0)} - \frac{1}{n(0)K_0} - \frac{K_0}{n(0)16} \right), \quad (18)$$

$$T_K = \frac{\hbar v_F \Lambda^*}{k_B} = \frac{\hbar v_F \Lambda_0}{k_B} \exp \left( \frac{1}{2n(0)} - \frac{1}{n(0)K_0} - \frac{K_0}{n(0)16} \right), \quad (19)$$

$$\xi_K = \frac{2\pi}{\Lambda^*} = \frac{\hbar v_F}{k_B T_K} = \frac{2\pi}{\Lambda_0} \exp \left( -\frac{1}{2n(0)} + \frac{1}{n(0)K_0} + \frac{K_0}{n(0)16} \right). \quad (20)$$

At the IR fixed point in the AF regime the effective Hamiltonian is given by,

$$H^* = \sum_{|\Lambda| < \Lambda^*} \hbar v_F \Lambda \hat{n}_{\Lambda, \hat{s}, \sigma} + \frac{J^*}{2} \sum_{\substack{j_1, j_2 < j^*, \\ m, m'}} \mathbf{S} \cdot c_{j_1, \hat{s}_m, \alpha}^\dagger \boldsymbol{\sigma}_{\alpha\beta} c_{j_2, \hat{s}_{m'}, \beta} + \sum_{j'=N, m=1}^{j^*, n_{j'}} J^{j'} S^z s_{j', m}^z, \quad (21)$$

where  $m$  refers to the various normal directions  $\hat{s}_m$  of the Fermi surface. In the above equation, the second term is the effective Hamiltonian for the coupling of the Kondo cloud to the impurity spin, while the third encodes the interaction between the impurity spin moment and the decoupled electronic degrees of freedom that do not belong to the Kondo cloud (lying on radial shells in momentum-space indexed by the RG step  $j$ ). When taken together with the first term (the kinetic energy/dispersion of the lattice conduction electrons), the third gives rise to the local Fermi liquid of Noziers. In this way, it can be viewed as a (mean-field)



self-energy for the decoupled electrons in the  $j'$  shell arising from their interaction with the impurity spin

$$\Sigma_{j'}^{dec} = J^{j'} \langle S^z \rangle . \quad (22)$$

As shown in Fig.4 (left panel), the local nature of the Fermi liquid can be seen by the rapid rise of the coupling  $J^j = 2K_j \epsilon_j$  with RG step/shell index  $j$  only very near to where the Kondo coupling saturates (signalling the Kondo cloud formation). For this plot, we chose  $\omega = \hbar v_F \Lambda_j$ , i.e., the energy cost for the spin-flip scattering of a single electron. We will see the exact derivation in detail in a subsequent section.

We can now extract a zero mode from the above Hamiltonian that captures the low energy theory near the Fermi surface,

$$\begin{aligned} H_{coll} &= \frac{1}{N} \sum_{|\Lambda| < \Lambda^*} \hbar v_F \Lambda \sum_{|\Lambda| < \Lambda^*} \hat{n}_{\Lambda, \hat{s}, \sigma} + \frac{J^*}{2} \sum_{\substack{j_1, j_2 < j^*, \\ m, m'}} \mathbf{S} \cdot c_{j_1, \hat{s}_m, \alpha}^\dagger \boldsymbol{\sigma}_{\alpha\beta} c_{j_2, \hat{s}_{m'}, \beta} + \sum_{j'=N, m=1}^{j, n_{j'}} J^{j'} S^z s_{j', m}^z \\ &= \frac{J^*}{2} \sum_{\substack{j_1, j_2 < j^*, \\ m, m'}} \mathbf{S} \cdot c_{j_1, \hat{s}_m, \alpha}^\dagger \boldsymbol{\sigma}_{\alpha\beta} c_{j_2, \hat{s}_{m'}, \beta} + \sum_{j'=N, m=1}^{j^*, n_{j'}} J^{j'} S^z s_{j', m}^z , \end{aligned} \quad (23)$$

where the first term vanishes as the sum over wavevector  $\Lambda$  within the symmetric window  $\Lambda^*$  around the Fermi surface itself vanishes.

Indeed, we observe that the zero mode Hamiltonian at the IR fixed point is responsible for the formation of the Kondo singlet ground state

$$|\Psi^*\rangle = \frac{1}{\sqrt{2}} \left[ |\uparrow\rangle \sum_{\Lambda, \hat{s}} |1_{\Lambda, \hat{s}, \downarrow}\rangle \otimes_{\Lambda' \neq \Lambda, \hat{s}' \neq \hat{s}} |\Lambda', \hat{s}'\rangle - |\downarrow\rangle \sum_{\Lambda, \hat{s}} |1_{\Lambda, \hat{s}, \uparrow}\rangle \otimes_{\Lambda' \neq \Lambda, \hat{s}' \neq \hat{s}} |\Lambda', \hat{s}'\rangle \right] . \quad (24)$$

Note that this state will be in direct product with the wavefunction for the decoupled electronic degrees of freedom.

#### **A. Variation of the Kondo cloud size $\xi_K$ and effective Kondo coupling $J^*$ as function of bare coupling $J_0$**

In Fig.5, we show the variation of the Kondo cloud size  $\xi_K$  and effective Kondo coupling  $J^*$  as function of bare coupling  $J$  (in units of  $t$ ) in the range  $5.7 \times 10^{-5} < J < 5.4$ . All plots below are obtained for momentum-space grid  $100 \times 100$  and with RG scale factor  $\Lambda_j = b \Lambda_{j+1}$  ( $b = 0.9999 = 1 - 1/N * N$ ,  $N = 100$ ). The  $E_F$  for the 2d tight binding band

$-W/2 < E_k = -2t(\cos k_x + \cos k_y) < W/2$  ( $W = 4t$ ) is chosen at  $E_F = -3.9t$ , and the bare  $k$ -space cutoff is set at  $\Lambda_0 \simeq 2.83$ .

The variation of the renormalised Kondo coupling  $J^*$  with the bare  $J$  shown in Fig.5 clearly indicates the flow under RG towards saturation at a strong coupling value of  $J_{sat}^* \sim 16$ . Similarly, the variation of the Kondo screening length  $\xi_K$  with  $J$  shows a fall to an asymptotic value of  $\xi_K \sim 3$  lattice sites at the strong coupling fixed point. We recall that Wilson's NRG calculation for the Kondo problem (for a bath of conduction electrons in the continuum with linear dispersion and a very large UV cutoff  $D$ ) shows that the renormalised Kondo coupling  $J^* \rightarrow \infty$  under flow to strong coupling. This can be reconciled from our URG results by noting that the value of  $J_{sat}^*$  increases upon rescaling the conduction bath bandwidth  $D$  to larger values (by rescaling the nearest neighbour hopping strength  $t$ ). This is shown in Fig.6, where we see that  $J_{sat}^*$  increases from a value of  $\mathcal{O}(1)$  (in units of  $t$ ) to  $\mathcal{O}(10^9)$  as  $t$  is increased from  $\mathcal{O}(1)$  to  $\mathcal{O}(10^4)$ . Thus, taking the limit of  $D \rightarrow \infty$  will lead to  $J_{sat}^* \rightarrow \infty$ .

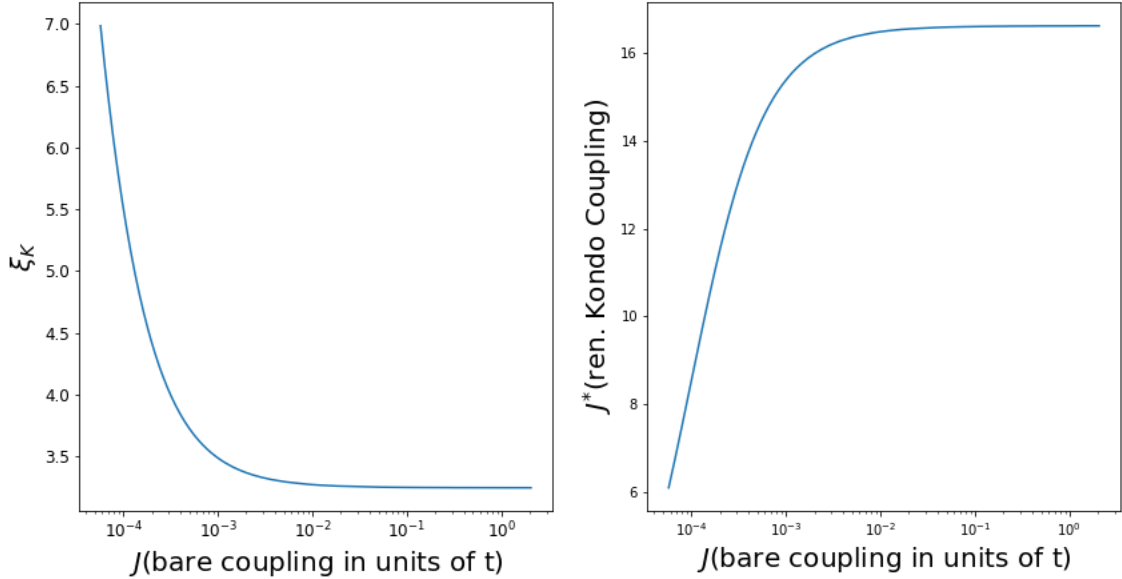


FIG. 5. Left panel: Kondo cloud length  $\xi$  vs. bare Kondo coupling  $J$  (x-axis in log scale) in , right panel: renormalized Kondo coupling  $J^*$  vs.  $J$  (x-axis in log scale). The bare Kondo coupling  $J$  is chosen to lie within the range  $5.7 \times 10^{-5} < J < 5.4$ .

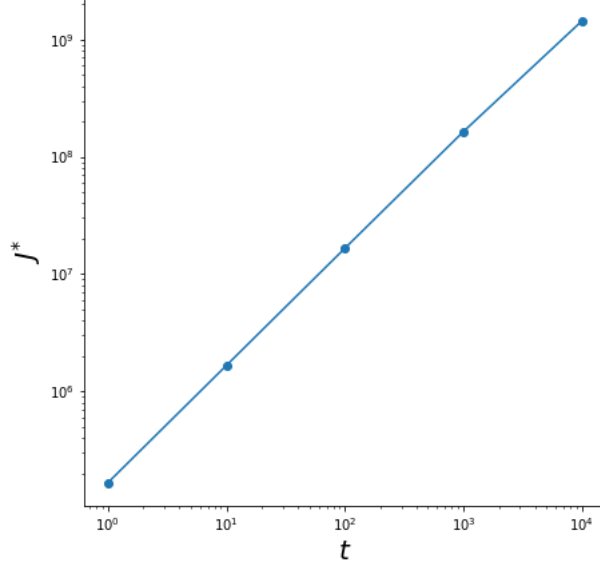


FIG. 6. Left panel: Variation of the renormalized Kondo coupling  $J^*$  with the hopping parameter  $\mathcal{O}(1) < t < \mathcal{O}(10^4)$  of the electronic bath (and hence the conduction band width).

#### IV. DERIVATION OF THE LOCAL FERMI LIQUID EFFECTIVE HAMILTONIAN

We begin by recalling the effective collective Hamiltonian obtained from the URG at the IR fixed point

$$H_{coll} = J^* \mathbf{S} \cdot \mathbf{s} + \sum_{l=N, m=1}^{j^*, n_l} J_l S^z s_{l,m}^z + \sum_{l=N, m=1}^{j^*, n_l} \epsilon_l (\hat{n}_{l,m,\uparrow} + \hat{n}_{l,m,\downarrow}) \quad (25)$$

The thermal density matrix at finite temperatures is then

$$\rho = \exp(-\beta H_{coll}) = \prod_{l=N, m=1}^{j^*, n_l} \exp(-\beta \epsilon_l (\hat{n}_{l,m,\uparrow} + \hat{n}_{l,m,\downarrow})) \times \exp(-\beta (J^* \mathbf{S} \cdot \mathbf{s} + \sum_{l=N, m=1}^{j^*, n_l} J_l S^z s_{l,m}^z)) \quad (26)$$

We now rewrite  $H_{coll}$  in the projected basis of the impurity spin and Kondo cloud ( $|\uparrow\downarrow\rangle, |\downarrow\uparrow\rangle$ )

$$\begin{aligned}
PH_{coll}P &= \begin{pmatrix} -\frac{J^*}{4} + \sum_{l=N,m=1}^{j^*,n_l} \frac{J_l}{2} s_{l,m}^z & \frac{J^*}{2} \\ \frac{J^*}{2} & -\frac{J^*}{4} - \sum_{l=N,m=1}^{j^*,n_l} \frac{J_l}{2} s_{l,m}^z \end{pmatrix} \\
&= -\frac{J^*}{4} + \sigma^z h_z + \frac{J^*}{2} \sigma_x = -\frac{J^*}{4} + A \boldsymbol{\sigma} \cdot \hat{\mathbf{n}}, \\
A &= \sqrt{h_z^2 + \frac{(J^*)^2}{4}}, \quad \cos \theta = \frac{h_z}{\sqrt{h_z^2 + \frac{(J^*)^2}{4}}}, \quad h_z = \sum_{l=N,m=1}^{j^*,n_l} \frac{J_l}{2} s_{l,m}^z. \quad (27)
\end{aligned}$$

Thus, the thermal density matrix can be rewritten as

$$\begin{aligned}
\rho &= \rho_0 \times \exp(-\beta(J^* \mathbf{S} \cdot \mathbf{s} + \sum_{l=N,m=1}^{j^*,n_l} J_l S^z s_{l,m}^z)) \\
&= \rho_0 \times \left[ 2 \exp(-\beta \frac{J^*}{4}) \cosh \left( \sum_{l=N,m=1}^{j^*,n_l} \frac{\beta J_l}{2} s_{l,m}^z \right) + \exp(\beta \frac{J^*}{4}) \exp(-\beta A \boldsymbol{\sigma} \cdot \hat{\mathbf{n}}) \right] \\
&= \rho_0 \times \left[ 2 \exp(-\beta \frac{J^*}{4}) \cosh \left( \sum_{l=N,m=1}^{j^*,n_l} \frac{\beta J_l}{2} s_{l,m}^z \right) + \exp(\beta \frac{J^*}{4}) [\cosh(\beta A) + \boldsymbol{\sigma} \cdot \hat{\mathbf{n}} \sinh(\beta A)] \right] \quad (28)
\end{aligned}$$

where  $\rho_0 = \prod_{l=N,m=1}^{j^*,n_l} \exp(-\beta \epsilon_l (\hat{n}_{l,m,\uparrow} + \hat{n}_{l,m,\downarrow}))$  is the thermal density matrix for the disentangled electrons.

In order to obtain the effective Hamiltonian for just the disentangled electrons, we trace out the impurity and Kondo cloud degrees of freedom from the thermal density matrix ( $\rho$ )

$$\begin{aligned}
\bar{\rho} &= Tr_{imp+cloud}(\rho) \\
&= Tr_{imp+cloud}(\rho_0 \times \exp(-\beta(J^* \mathbf{S} \cdot \mathbf{s} + \sum_{l=N,m=1}^{j^*,n_l} J_l S^z s_{l,m}^z))) \\
&\approx \rho_0 \times \exp(\beta \frac{J^*}{4}) \exp(\beta A), \quad \text{for } \beta \rightarrow \infty \quad (29)
\end{aligned}$$

Thus, we obtain the effective Hamiltonian for the disentangled electrons

$$\begin{aligned}
H_{eff} &= -k_B T \log(Tr_{imp+cloud}(\exp(-\beta H_K^*))) \approx \sum_{l,m} \epsilon_l (\hat{n}_{l,m,\uparrow} + \hat{n}_{l,m,\downarrow}) - \frac{J^*}{4} - \frac{J^*}{2} \sqrt{1 + \frac{4h_z^2}{(J^*)^2}} \\
&\approx \sum_{l,m} \epsilon_l (\hat{n}_{l,m,\uparrow} + \hat{n}_{l,m,\downarrow}) - \frac{3J^*}{4} - \frac{h_z^2}{J^*}, \quad (30)
\end{aligned}$$

where we recall that  $h_z = \sum_{l=N,m=1}^{j^*,n_l} \frac{J_l}{2} s_{l,m}^z$  contains spin density density interactions between the disentangled electrons of various shells  $\Lambda \geq \Lambda^*$ . Importantly, we see that the ground state

energy of the Kondo singlet ( $-3J^*/4$ ) appears, signalling that  $H_{eff}$  governs the dynamics of quasiparticle excitations.

Now, upon expanding the square root term within  $H_{eff}$  in leading orders of  $\frac{\hbar^z}{J^*}$ , we obtain the Fermi liquid fixed point theory

$$H_{FL} = \sum_{l,m} \epsilon_l (\hat{n}_{l,m,\uparrow} + \hat{n}_{l,m,\downarrow}) - \sum_{l,l',m,m'} f_{ll'} s_{l,m}^z s_{l',m'}^z, f_{ll'} = \frac{J_l J_{l'}}{J^*}, s_{l,m}^z = \frac{1}{2} (\hat{n}_{l,m,\uparrow} - \hat{n}_{l,m,\downarrow}) \quad (31)$$

Given that the interaction strength  $f_{ll'} = \frac{J_l J_{l'}}{J^*}$  falls off sharply compared to  $\epsilon_{\Lambda^*}$  with increasing distances  $\Lambda > \Lambda^*$  (see left panel of Fig.4) with the highest magnitude being that for electronic states on shell  $\Lambda^*$  ( $f_{j^*} = J_* = 4\epsilon_{\Lambda^*}$ ), we obtain the “local” Fermi liquid Hamiltonian for the disentangled electrons of the shell  $\Lambda^*$  as

$$H_{LFL} = \epsilon_* \sum_m (\hat{n}_{*,m,\uparrow} + \hat{n}_{*,m,\downarrow}) - J^* \sum_{m,m'} s_{*,m}^z s_{*,m'}^z = \frac{1}{2} (\hat{n}_{\Lambda^*,m,\uparrow} - \hat{n}_{\Lambda^*,m,\downarrow}) . \quad (32)$$

### A. Wilson ratio ( $R$ ) for the local Fermi liquid

By following the steps shown in Refs.[11, 16], we now obtain the Wilson ratio for the local Fermi liquid we have derived above. For this, we note that the energy cost for quasiparticle excitations with density  $\delta n_{*,m,\sigma}$  is given by

$$\mathcal{E} = \mathcal{E}_0 + \epsilon_* \sum_{m,\sigma} \delta n_{*,m,\sigma} + \frac{J^*}{4} \sum_{m,m',\sigma} \delta n_{*,m,\sigma} \delta n_{*,m',-\sigma} + \frac{J^*}{4} \sum_{m,m',\sigma} n_{*,m,\sigma} \delta n_{*,m',-\sigma} . \quad (33)$$

Then, it is easily seen that

$$\begin{aligned} \frac{\delta \mathcal{E}}{\delta n_{*,m,\sigma}} &= \epsilon_* + \frac{J^*}{4} \sum_{m'} \delta n_{*,m',-\sigma} + \frac{J^*}{4} \sum_{m'} n_{*,m',-\sigma} , \\ &= \epsilon_* + \frac{\Delta \epsilon}{\pi} \delta_\sigma(\{n_{*,m',-\sigma}\}, \epsilon_*) , \end{aligned} \quad (34)$$

where we have taken

$$\begin{aligned} E_k - E_F &= -2t \cos(k_{Fx} + \Lambda^*) - 2t \cos(k_{Fy} + \Lambda^*) + 2t \cos k_{Fx} + 2t \cos k_{Fy} \\ &= 2t (\sin k_{Fx} + \sin k_{Fy}) \Lambda^* \approx 2t (k_{Fx} + k_{Fy}) \Lambda^* . \end{aligned} \quad (35)$$

Therefore, we obtain

$$\frac{\Delta E}{\Delta \Lambda^*} = 2t (k_{Fx} + k_{Fy}) , \quad \Delta \epsilon = 2t (k_{Fx} + k_{Fy}) \frac{\pi}{L} . \quad (36)$$

This leads to the quasiparticle (Friedel's) scattering phase shift

$$\delta_\sigma(\{n_{*,m',-\sigma}\}, \epsilon_*) = \frac{\pi J^*}{4\Delta\epsilon} \sum_{m'} \delta n_{*,m',-\sigma} + \frac{\pi}{2} + \alpha(\epsilon_* - E_F) , \quad (37)$$

where  $\delta_0 = \frac{\pi}{2}$  is the phase shift accounting for the absorption of an effective single electron (corresponding to the Kondo cloud) into the singlet. The quantity  $\alpha(\epsilon_* - E_F) = \frac{\pi J^*}{4\Delta\epsilon} \sum_{m'} n_{*,m',-\sigma} - \frac{\pi}{2}$  accounts for the quasiparticle self energy generated by potential scattering with the impurity-cloud singlet [11, 16, 17]. Following Ref.[11, 16], we obtain the zero temperature specific heat coefficient (in units of  $k_B = 1$ ) as

$$\gamma = \frac{2\pi}{3} \alpha(\epsilon_* - E_F) , \quad (38)$$

and the impurity spin susceptibility as

$$\chi = \frac{4\alpha(\epsilon_* - E_F)}{\pi} . \quad (39)$$

This leads to Wilson's ratio ( $R$ )

$$R = \frac{\chi}{\gamma} \frac{\pi^2}{3} = 2 . \quad (40)$$

## V. IMPURITY SUSCEPTIBILITY AT FINITE TEMPERATURES

The complete effective Hamiltonian for the impurity spin ( $\mathbf{S}$ ), Kondo cloud spin ( $\mathbf{s}$ ) and the electrons that comprise the local Fermi liquid has the form,

$$H_2 = \epsilon_* \sum_{m,\sigma} \hat{n}_{*,m,\sigma} + J^* \mathbf{S} \cdot \mathbf{s} + J^* S^z \sum_m s_{*,m}^z . \quad (41)$$

The Hamiltonian  $H_2$  has several conserved quantities which we depict below,

$$[H_2, S^z + s^z] = 0 , \quad [H_2, s_{*,m}^z] = 0 \quad \forall \quad 1 \leq m \leq n_j , \quad (42)$$

such that  $[H^*, S_{tot}^z] = 0$  where  $S_{tot}^z = S^z + s^z + \sum_m s_{*,m}^z$ . Therefore, the eigenvalues of  $|s_{*,m}^z = \uparrow / \downarrow\rangle$  are good quantum numbers; this is simply an outcome of the URG method. We can now extract the effective Kondo impurity-electron cloud Hamiltonian by treating the effect of local Fermi liquid electrons as an effective field  $B = J^* \sum_m \langle s_{*,m}^z \rangle$  (note that this the eigenvalue of the LFL spins) on the impurity spin,

$$H_K^* = J^* \mathbf{S} \cdot \mathbf{s} + B S^z . \quad (43)$$

It is also important to note that the URG procedure did not lead to the generation of spin density density interaction between the electrons of the Kondo cloud and those of the LFL. We now obtain the impurity magnetization and susceptibility from this effective Hamiltonian. The four state eigenspectrum of  $H_K^*$  is given by

$$\begin{aligned} E_1 &= \frac{1}{2}(-\frac{J^*}{2} + \sqrt{B^2 + J^{*2}}) , \quad E_2 = \frac{1}{2}(-\frac{J^*}{2} - \sqrt{B^2 + J^{*2}}) , \\ E_3 &= E_4 = \frac{J^*}{4} . \end{aligned} \quad (44)$$

The partition function for this Hamiltonian (with  $\beta = \frac{1}{k_B T}$ ) is given by

$$Z(B) = 2 \exp(\beta \frac{J^*}{4}) \left[ \cosh(\beta \frac{B}{2}) + \cosh(\frac{\beta}{2}(\sqrt{B^2 + J^{*2}})) \right] . \quad (45)$$

The magnetization is then given by,

$$M = \frac{k_B T}{Z(B)} \frac{dZ(B)}{dB} = \frac{k_B T}{Z(B)} \exp(\beta \frac{J^*}{4}) \beta \left[ \sinh(\beta \frac{B}{2}) + \frac{B}{\sqrt{B^2 + J^{*2}}} \sinh(\frac{\beta}{2} \sqrt{B^2 + J^{*2}}) \right] \quad (46)$$

and the susceptibility is obtained by taking the effective field  $B \rightarrow 0$

$$\chi = \lim_{B \rightarrow 0} \frac{dM}{dB} = \frac{\frac{\beta}{4} + \frac{1}{2J^*} \sinh(\frac{\beta}{2} J^*)}{1 + \cosh(\frac{\beta}{2} J^*)} . \quad (47)$$

We can now make several important observations based on eq.47. First, the saturation value of  $4T_K \chi$  as  $\beta \rightarrow \infty$  (i.e.,  $T \rightarrow 0$ ) is given by

$$\chi(T=0) = \frac{1}{2J^*} . \quad (48)$$

We find that the Wilson number  $W = 4T_k \chi(T=0) = \frac{2T_k}{J^*}$ . For values of  $J^* \simeq 16.612t$  and  $T_k \simeq 3.433t$  we obtain  $W = 0.413$ . This is in excellent agreement with the value for  $W$  obtained from NRG [8] and Bethe Ansatz solution of the Kondo problem [5, 6]. This is shown in Fig.7 (upper panel). Further, we show the variation of  $W$  with the bare Kondo coupling  $J$  in Fig.7 (lower panel). The figure clearly shows the saturation of  $W$  to the value mentioned above as  $J$  flows to the strong coupling fixed point.

Second, the  $T_k \chi$  vs temperature curve shown in Fig.7 has a non-monotonic behaviour, i.e., we find a maxima obtained from the transcendental equation

$$\begin{aligned} \frac{d\chi}{d\beta} &= \frac{1}{4} - \frac{1}{4} \frac{(1 + \frac{2}{J^* \beta} \sinh \frac{\beta J^*}{2})(\frac{J^* \beta}{2} \sinh \frac{\beta J^*}{2})}{(1 + \cosh \beta \frac{J^*}{2})^2} \\ \implies (1 + \cosh \beta \frac{J^*}{2})^2 &= \frac{J^* \beta}{2} \sinh \frac{\beta J^*}{2} + \sinh^2 \frac{\beta J^*}{2} . \end{aligned} \quad (49)$$

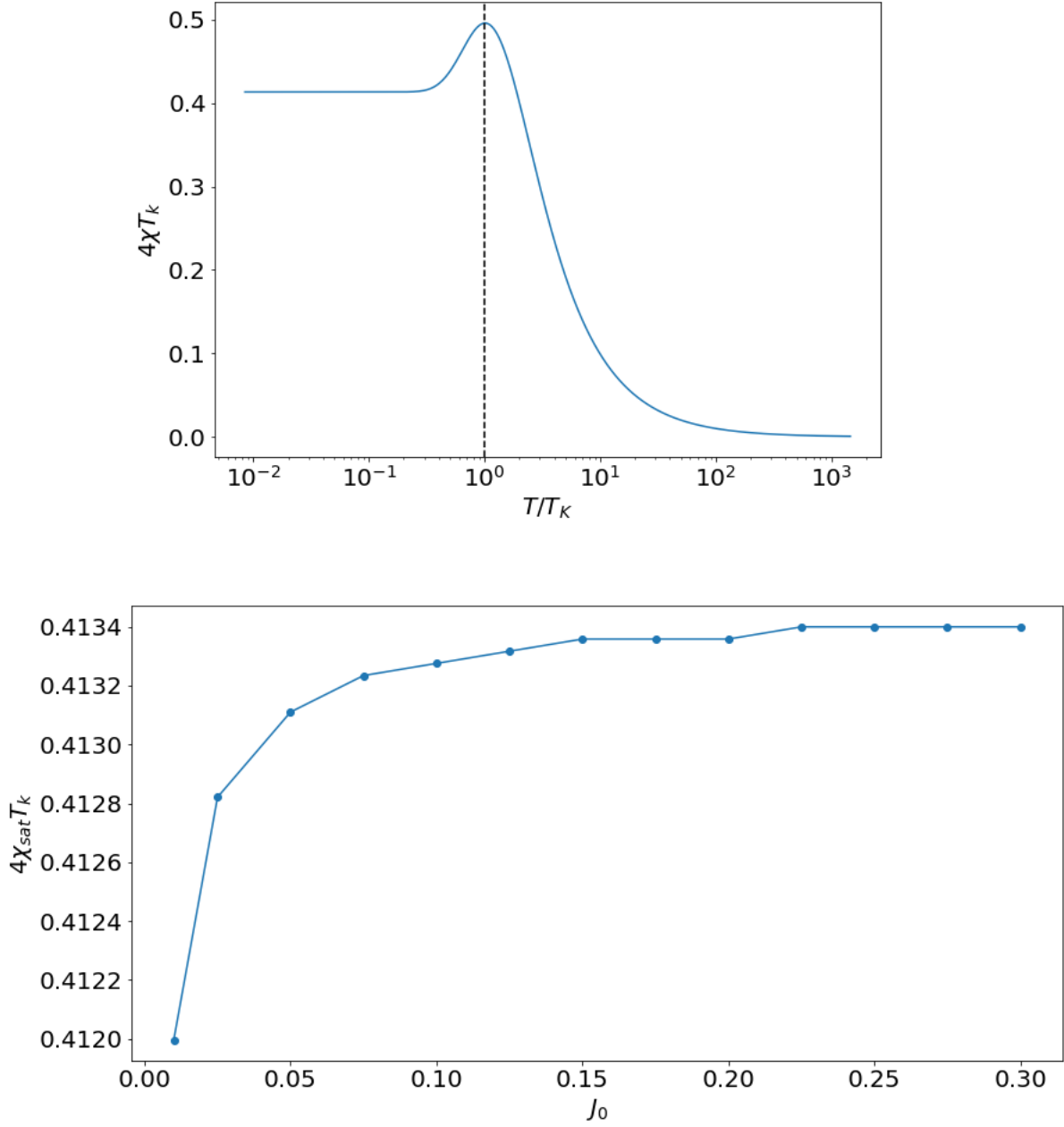


FIG. 7. Upper panel: Variation of  $4T_K\chi$  with  $T/T_K$ . Dashed line shows  $T = T_K$ . Lower panel: Variation of Wilson number  $W$  with bare Kondo coupling  $J_0$ . See discussion in text.

We confirm from our numerical studies that the temperature ( $T_{max}$ ) corresponding to the maximum value of  $T_K\chi$  varies as  $T_{max} \rightarrow T_k$  as  $J$  flows to strong coupling. Further, we find that the maximum value of  $T_K\chi$  does not vary with the bare  $J$  in the range  $\mathcal{O}(10^{-5}) <$



$J < \mathcal{O}(1)$ . We note that such a maxima is not obtained from NRG treatments of the Kondo problem. We speculate that this discrepancy between the results of NRG and URG may likely stem from the fact that our present URG analysis has kept only the leading contributions from the Kondo scattering vertex and neglected all higher-order scattering vertices (see discussion below eq.(9)). This may also be a result of the difference in the nature of the two RG methods, NRG is in projective while URG is unitary. This will, however, need a more careful comparative study.

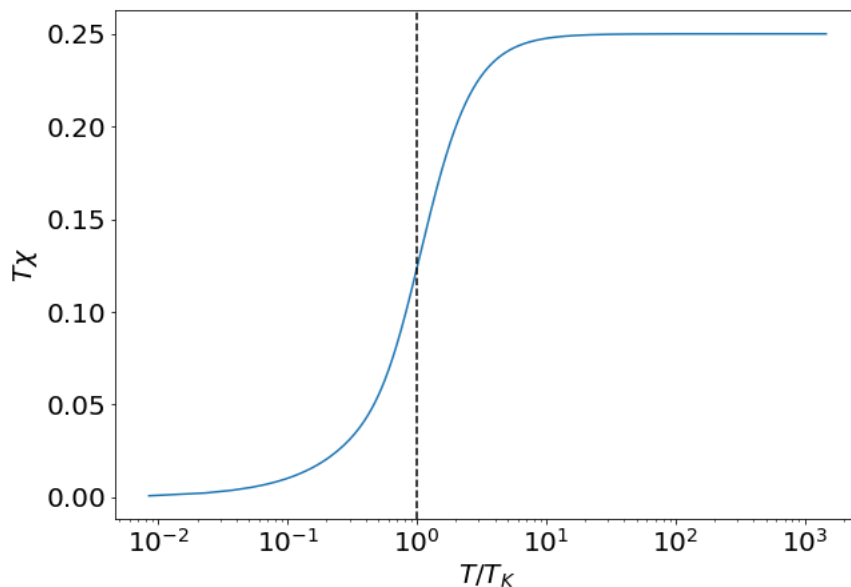


FIG. 8. Variation of  $T\chi$  with  $T/T_K$ . See discussion in text.

Finally, we find that the saturation value of  $T \times \chi$  for  $\beta \rightarrow 0$  is given by the universal value

$$k_B T \chi(T = \infty) = \frac{1}{4}, \quad (50)$$

as shown in Fig.8. The saturation value at high- $T$  arises from the Ising coupling of the disentangled conduction electrons with the impurity spin (the third term in eq.(41)) and reflects the physics of the (almost isolated) local impurity spin moment, while the vanishing value of  $T\chi$  originates from the formation of the singlet between the Kondo cloud and the impurity spin (second term in eq.(41)). Following our discussion in an earlier chapter of the fact that the finite temperature partition function can be obtained from the IR stable fixed point Hamiltonian (see eq.(11)), it is not surprising that Fig.8 displays the entire crossover

of the RG flow from the local moment regime at high- $T$  to the screened singlet regime at low- $T$ .

## VI. EXCITATIONS OF THE KONDO CLOUD AND THE SOMMERFIELD CO-EFFICIENT

In this section we will study the effect of the renormalized Kondo coupling on the self energy of the electrons comprising the Kondo cloud. We integrate out the decoupled electronic states to obtain the effective Hamiltonian  $H^*$  of the impurity + electronic cloud system. In this Hamiltonian we have additionally kept the electronic dispersion to study the effect of electronic density fluctuation due to the inter-electronic interaction mediated by the impurity spin,

$$H^* = H_0^* + \frac{J^*}{2} \sum_{\substack{j_1, j_2 < j^*, \\ m, m'}} \mathbf{S} \cdot c_{j_1, \hat{s}_m, \alpha}^\dagger \boldsymbol{\sigma}_{\alpha\beta} c_{j_2, \hat{s}_{m'}, \beta} \quad (51)$$

$$H_0^* = \sum_{|\Lambda_j| < \Lambda^*, \sigma} \epsilon_j \hat{n}_{j, \hat{s}, \sigma} . \quad (52)$$

In order to study the inter-electronic interaction we need to isolate the quantum impurity from the Kondo cloud. This can be done by first recasting the many body eigenstate  $|\Psi\rangle$  of  $H^*$  in the  $\uparrow / \downarrow$  basis of the impurity and the associated configuration of the rest electronic states,

$$|\Psi\rangle = a_0 |\uparrow_{imp}\rangle |\Phi_0\rangle + a_1 |\downarrow_{imp}\rangle |\Phi_1\rangle, \quad (53)$$

here  $|\Phi_0\rangle$  and  $|\Phi_1\rangle$  refer to the electronic configurations of the remnant electrons. With the above decomposed state we can rewrite the eigen value relation for  $H_K^*$  as a set of two coupled equations ( $E_1$  is the eigenvalue),

$$\begin{aligned} a_0(H_0^* + \frac{J^*}{2}s_z)|\Phi_0\rangle + a_1\frac{J^*}{2}s_+|\Phi_1\rangle &= a_0E_1|\Phi_0\rangle \\ a_0\frac{J^*}{2}s_-|\Phi_0\rangle + a_1(H_0^* - \frac{J^*}{2}s_z)|\Phi_1\rangle &= a_1E_1|\Phi_1\rangle . \end{aligned} \quad (54)$$

Combining this two equations we can obtain,

$$a_0(\frac{J^*}{2}s_z)|\Phi_0\rangle + s_+\frac{\frac{(J^*)^2}{4}}{E + \frac{J^*}{2}s_z - H_0^*}s_-|\Phi_0\rangle = a_0(E - H_0^*)|\Phi_0\rangle \quad (55)$$

From here we obtain the form of the effective Hamiltonian accounting for the leading order density-density and off-diagonal four Fermi interaction terms,

$$\begin{aligned}
H_{eff} &= \frac{J^*}{2} s_z + s_+ \frac{\frac{(J^*)^2}{4}}{(E_1 + \frac{J^*}{2} s_z)(1 - \frac{1}{E_1 + \frac{J^*}{2} s_z} H_0^*)} s_- \\
&\approx \frac{J^*}{2} s_z + s_+ \frac{\frac{(J^*)^2}{4}}{E_1 + \frac{J^*}{2} s_z} (1 + \frac{1}{E_1 + \frac{J^*}{2} s_z} H_0^* + \frac{1}{E + \frac{J^*}{2} s_z} H_0^* \frac{1}{E + \frac{J^*}{2} s_z} H_0^*) s_- + O((H_0^*)^3) \\
&\approx \frac{J^*}{2} s_z + s_+ \frac{\frac{(J^*)^2}{4}}{E + \frac{J^*}{2} s_z} s_- + s_+ \frac{\frac{(J^*)^2}{4}}{(E_1 + \frac{J^*}{2} s_z)^2} H_0^* s_- + s^+ \frac{\frac{(J^*)^2}{4}}{(E_1 + \frac{J^*}{2} s_z)^2} H_0^* \frac{1}{E + \frac{J^*}{2} s_z} H_0^* s_-, \\
&\approx \frac{J^*}{2} s_z + (\frac{1}{2} + s_z) \frac{\frac{(J^*)^2}{4}}{E_1 - \frac{J^*}{2} s_z} + s_+ \frac{\frac{(J^*)^2}{4}}{(E_1 + \frac{J^*}{2} s_z)^2} (s_- H_0^* + [H_0^*, s_-]) + \\
&\quad + s_+ \frac{\frac{(J^*)^2}{4}}{(E_1 + \frac{J^*}{2} s_z)^2} H_0^* \frac{1}{E_1 + \frac{J^*}{2} s_z} (s_- H_0^* + [H_0^*, s_-]) . \tag{56}
\end{aligned}$$

Finally we obtain the effective Hamiltonian upon setting  $E_1 = 0$  in the equation above and choosing  $s_z = \frac{1}{2}$  (this is the spin configuration associated with the wave function eq.(53) in eq.(55), from which the effective Hamiltonian is derived),

$$H_{eff} = -\frac{3J^*}{4} + 4(H_0^* + H_0^* \frac{4}{J^*} H_0^*) + \sum_{k_1, k_2, k_3, k_4} \frac{4\epsilon_k \epsilon_{k_1}}{J^*} c_{k_4\uparrow}^\dagger c_{k\downarrow}^\dagger c_{k_2\downarrow} c_{k_1\uparrow} . \tag{57}$$

The first represents the ground state energy of the singlet configuration, the second term the kinetic energy (eq.(52)) density-density correlation (see eq.(58) below), and the third term the spin-fluctuation mediated electron-electron scattering process respectively.

In order to study the thermodynamic properties of the Fermi liquid we restrict our attention to the density-density terms only, at a later point we will see the effect of non-Fermi liquid corrections due to the off-diagonal terms. From the density terms we obtain the low excitation energy functional accounting for the quasiparticle interaction

$$E = E_0 + \sum_{\mathbf{k}\Lambda\hat{s}, \Lambda < \Lambda^*} \epsilon_{\mathbf{k}} \delta n_{\mathbf{k}\sigma} + \sum_{\mathbf{k}, \mathbf{k}'} \frac{4\epsilon_{\mathbf{k}} \epsilon_{\mathbf{k}'}}{J^*} \delta n_{\mathbf{k}\sigma} \delta n_{\mathbf{k}'\sigma'} . \tag{58}$$

This leads to the renormalized one-particle dispersion, where the self energy term has the following form

$$\bar{\epsilon}_\Lambda = \epsilon_\Lambda + \Sigma_\Lambda, \Sigma_\Lambda = (\sum_{\Lambda', \hat{s}, \sigma'} \frac{4\epsilon_{\Lambda'} \epsilon_{\Lambda'}}{J^*} \delta n_{\Lambda', \hat{s}, \sigma'}) \text{ for } \Lambda < \Lambda^* . \tag{59}$$

Note that as  $\Lambda \rightarrow 0$ ,  $\Sigma_\Lambda \rightarrow 0$ . Next, we compute the specific heat of the impurity from the Fermi Dirac distribution of the renormalized quasiparticles

$$\begin{aligned} C_{imp} &= C(J^*) - C(0) \\ &= \sum_{\Lambda, \delta, \sigma} \left( \frac{(\bar{\epsilon}_\Lambda)^2 \exp(\beta \bar{\epsilon}_\Lambda)}{(\exp(\beta \bar{\epsilon}_\Lambda) + 1)^2} - \frac{(\epsilon_\Lambda)^2 \exp(\beta \epsilon_\Lambda)}{(\exp(\beta \epsilon_\Lambda) + 1)^2} \right), \end{aligned} \quad (60)$$

where  $C(J^*)$  is the specific heat for the electronic system with the Kondo impurity, and  $C(0)$  is the specific heat for the free electronic system without coupling to Kondo impurity. The specific heat coefficient is given by  $\gamma_{imp} = \frac{C_{imp}}{k_B T}$ . Fig.9(left panel) shows that  $\gamma_{imp} T_K$  rises from 0 at high temperatures  $T > 10^2 T_K$  and saturates at a value  $\gamma_{imp}(0) T_K = 0.0519$  for  $T < 10^{-2} T_K$ . The Wilson ratio in Fig.9(right panel) obtained from the ratio of the saturation values of the susceptibility and specific heat coefficient saturates to a value  $W = \chi(0)/\gamma_{imp}(0) = 2.012$  for  $T < 10^{-2} T_K$ .

## VII. MANY BODY CORRELATIONS AND ENTANGLEMENT PROPERTIES OF THE KONDO CLOUD

In order to study the effect of the off-diagonal terms eq.(57) on the constituents of the Kondo cloud we perform a reverse URG treatment (shown in Fig.11) starting from the Kondo model ground state  $|\Psi^*\rangle$  at the IR fixed point eq.(24).

For the present study we take a toy model construction of the ground state wavefunction  $|\Psi^*\rangle$  eq.(24) at IR, the Kondo impurity couples to 12 electronic states  $|\mathbf{k}\sigma\rangle$  of which three are occupied and 9 are unoccupied. The net spin of the electrons comprising the Kondo cloud is oppositely aligned to that the Kondo impurity. The Kondo cloud system is in tensor product with 14 separable electronic states. This construction is represented in Fig.10 At each URG step  $U_{j,\uparrow} U_{j,\downarrow}$  two electronic states  $|k_j, \uparrow\rangle, |k_j, \downarrow\rangle$  are disentangled in reaching the IR fixed point. Upon performing reverse RG at each step two electrons are re-entangled into the eigenstates via the inverse unitary maps  $U_{j,\uparrow}^\dagger U_{j,\downarrow}^\dagger$ , Fig.11, all total we perform seven reverse RG steps. This reverse RG program is numerically implemented using python.

We use the wavefunctions generated under the reverse RG to compute the mutual information between (a) an electron in the Kondo cloud and the impurity electron, and (b) two electrons within the cloud. MI measures the total amount of quantum and classical

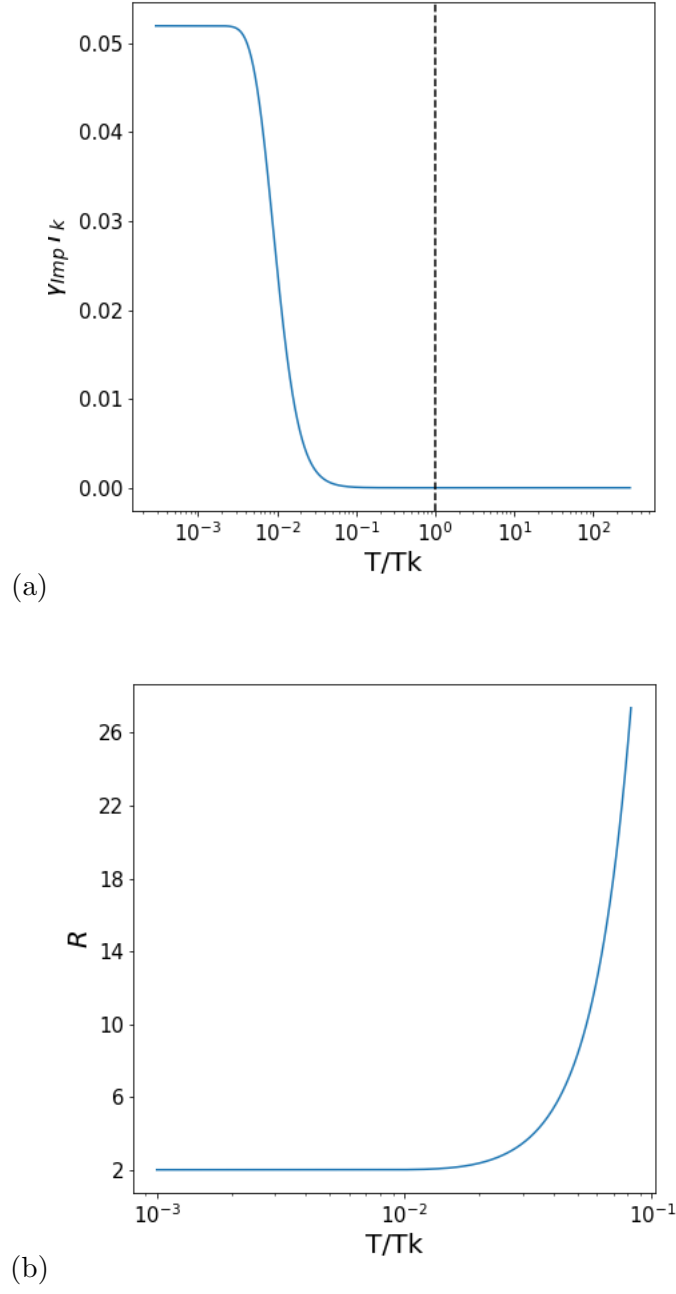


FIG. 9. (a) Variation of  $\gamma_{imp} T_K$  with  $T/T_K$ , dashed line shows  $T = T_k$ . (b) Variation of  $R$  Wilson ratio with  $T/T_K$ .

correlations in a system [18]. The mutual information between two electrons is given by

$$I(i : j) = -Tr(\rho_i \ln \rho_i) - Tr(\rho_j \ln \rho_j) + Tr(\rho_{ij} \ln \rho_{ij}) , \quad (61)$$

where  $\rho_i$  or  $\rho_j$  and  $\rho_{ij}$  are the 1- and 2-electron reduced density matrices respectively ob-

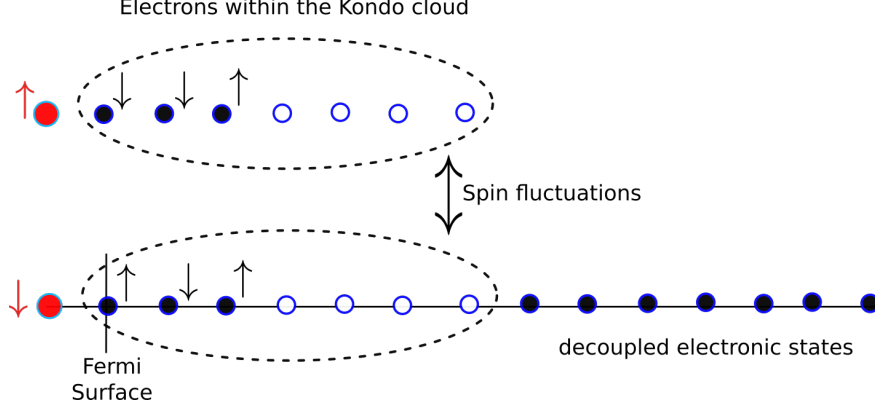


FIG. 10. Figure describes the electronic Kondo cloud (dashed oval) coupled to the impurity spin (red arrow).

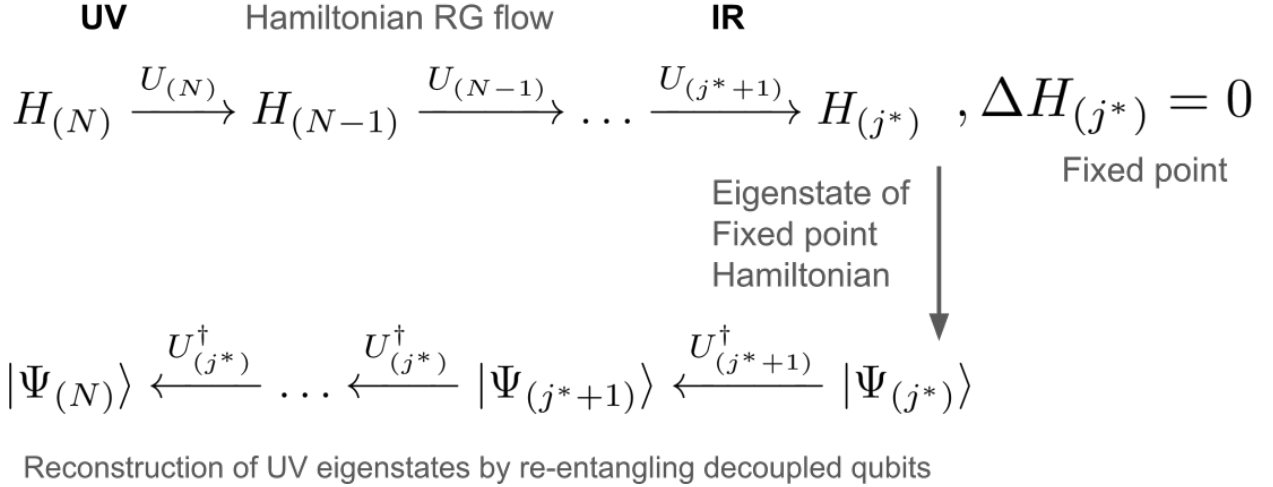


FIG. 11. The first line represent the Hamiltonian RG flow via the unitary maps. Upon reaching the Kondo IR fixed point, reverse RG will re-entangled decoupled electronic states with the Kondo singlet. This will result in generation of the many body eigenstates at UV.

tained from the wavefunctions obtained at each step of the reverse RG simulation. In Fig.12, we present the RG flow of both types of mutual information mentioned above. The orange curve in Fig.12(a) represents the plot for the maximum mutual information  $I(e : e)$  (eq.(61)) between any two of the electrons comprising the Kondo cloud, and shows that the maximum entanglement content/quantum correlation increases under RG flow from UV to IR. This implies that the electrons within the Kondo cloud is not simply a separable state in momentum space expected of a local Fermi liquid. This is a strong indication of the fact

that the two-particle off-diagonal  $(c_{k_4\uparrow}^\dagger c_{k\downarrow}^\dagger c_{k_2\downarrow} c_{k_1\uparrow})$  scattering term in eq.(57) is playing a role in the electronic entanglement within the Kondo cloud. Further, the blue curve in Fig.12(a) shows that the maximum mutual information between the Kondo impurity and any one member of the electronic cloud also increases under RG and to a higher value compared to that between electrons. This originates from the maximally entangled singlet state that is formed between the impurity and the electronic cloud. In this manner, the Kondo impurity mediates the entanglement between electrons (orange curve) in the Kondo cloud.

In order to understand this further, we also study (i) the maximum density-density correlations  $\max_{k,k_1} \langle \hat{n}_{k\uparrow} \hat{n}_{k_1\downarrow} \rangle$  (blue curve in Fig.12(b)), and (ii) the maximum two-particle off-diagonal correlations  $\max_{k,k_1} \langle c_{k\uparrow}^\dagger c_{k_1\downarrow}^\dagger c_{k_2\downarrow} c_{k_3\uparrow} \rangle$  (orange curve in Fig.12(b)) between electrons within the Kondo cloud. The plots show clearly that both the correlations grow under RG from UV to IR, finally reach the same value at the IR fixed point. Given that the amplitude of the number diagonal term in the effective Hamiltonian for the Kondo cloud  $(\frac{4\epsilon_k \epsilon_{k_1}}{J^*}, \text{eq.(57)})$  is much smaller than that for the decoupled electronic degrees of freedom  $(\frac{J^*}{4}, \text{eq.(33)})$  at strong coupling  $(J^* \gg 1)$ , we see that the local Fermi liquid is formed predominantly by the latter. On the other hand, the large values of the off-diagonal correlations reinforce our observation of a non-zero mutual information content between the cloud electrons. This implies that the electronic cloud is, in general, a non-Fermi liquid with non-zero entanglement content. Further studies of the many body entanglement content and transport properties are required to understand the physics of these non-Fermi liquid metal.

## VIII. CONCLUSIONS

The Kondo problem [1] is one of the oldest and well studied problem of electronic correlations in condensed matter [4, 7], and represents a set of benchmarking exercises for verifying the accuracy of the URG method. The RG analysis of the Kondo Hamiltonian leads to a zero temperature phase diagram revealing a intermediate coupling fixed point for an antiferromagnetic Kondo coupling. At the IR fixed point, we obtained the effective Hamiltonian, the ground state wavefunction and the energy eigenspectrum. This enabled the computation of various thermodynamic quantities such as the impurity susceptibility, specific heat coefficient, Wilson ratio, Wilson number, all of which are found to be in excellent agreement

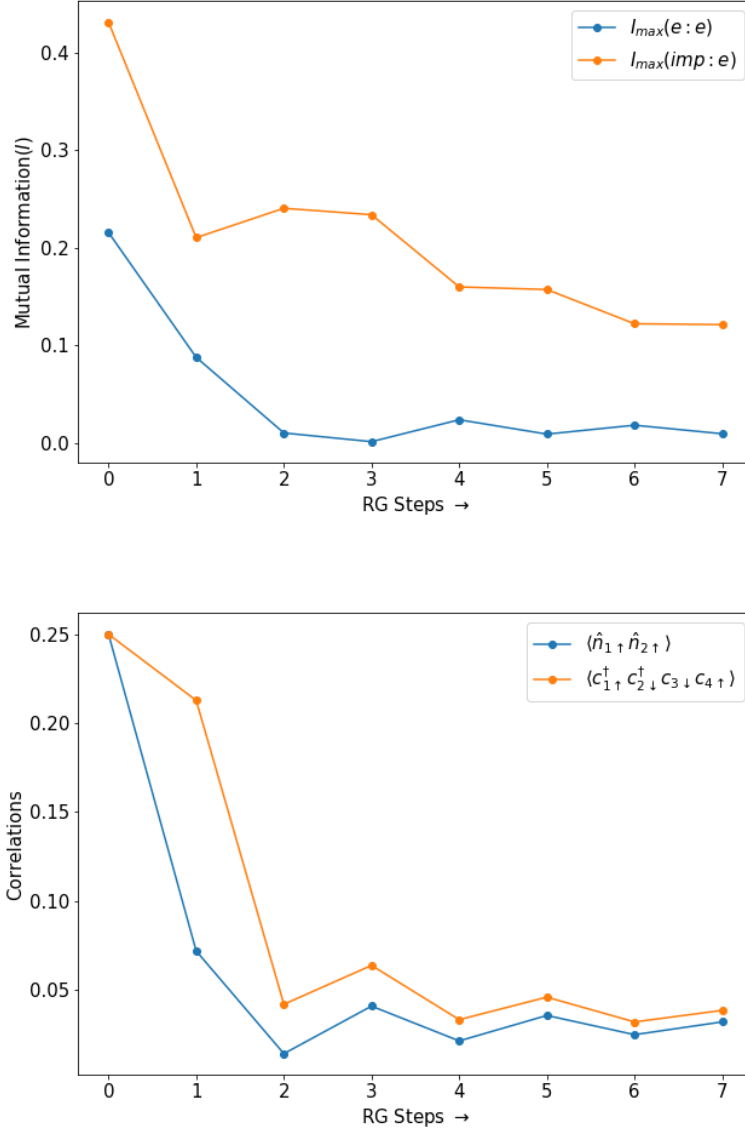


FIG. 12. Figure(a) shows the RG flows for the maximum mutual information between the impurity and electron (orange curve) and diagonal correlations (blue curve). Figure(b) shows the RG flows for the off-diagonal (orange curve) and diagonal correlations (blue curve).

with that obtained from the NRG studies [8]. It is also important to appreciate that we were able to capture the entire RG (crossover) flow at finite temperatures from the complete effective Hamiltonian (eq.(41)) obtained upon reaching the IR stable fixed point (as seen, for instance, for the susceptibility  $\chi(T)$  in Fig.8). As the URG relies purely on unitary



transformations, the eigenspectrum is preserved under the RG flow, and thence so is the partition function. Thus, at each RG fixed point, the effective Hamiltonian eq.(41) enables the construction of the density matrix for a given temperature scale  $k_B T$ , such that one can compute the finite temperature partition function (eq.(11)).

Furthermore, we found that the effective Hamiltonian for the Kondo cloud, obtained by integrating out the impurity spin, contains a density-density repulsion (corresponding to the local Fermi liquid) as well as a four-fermion interaction term description. In order to understand the roles of the two types of electronic correlations better, we performed a comparative study of the RG evolution of four-point number diagonal and number off-diagonal correlators. By using the singlet IR ground state wavefunction obtain from the URG analysis, we also studied the RG evolution of the mutual information (an entanglement based measure) between (a) the impurity and an electron in the cloud and (b) two electrons in the cloud. The results show strong inter-electronic as well as electron-impurity entanglement upon approaching the IR fixed point. This is in agreement with the presence of both types of two-particle correlators at the IR ground state. We find that both the number diagonal and number off-diagonal correlators reach same value at the IR fixed point, indicating that the electronic configuration within the Kondo cloud is not simply a local Fermi liquid. Indeed, our analysis lays bare the fact that the local Fermi liquid is formed primarily from the decoupled electrons lying outside the cloud, while the large entanglement within the Kondo cloud is an indication of the spin singlet it forms together with the impurity spin. Future studies need to be performed for investigating the nature of the correlated non-Fermi liquid metal comprising the Kondo cloud, e.g., various observables like spectral function, resistivity of the electronic system need to be quantified. Such studies should help in providing predictions that can be tested experimentally.

## CALCULATION OF EFFECTIVE HAMILTONIAN FROM URG

Starting from the Kondo Hamiltonian eq.(1) and using the URG based Hamiltonian RG equation eq.(10), we obtain the renormalised Hamiltonian

$$\begin{aligned}
\Delta \hat{H}_{(j)} = & \sum_{\substack{m=1, \\ \beta=\uparrow/\downarrow}}^{n_j} \frac{(J^{(j)})^2 \tau_{j,\hat{s}_m,\beta}}{2(2\omega\tau_{j,\hat{s}_m,\beta} - \epsilon_{j,l}\tau_{j,\hat{s}_m,\beta} - J^{(j)}S^z s_{j,\hat{s}_m}^z)} \\
& \times \left[ S^a S^b \sigma_{\alpha\beta}^a \sigma_{\beta\gamma}^b \sum_{\substack{(j_1,j_2 < j), \\ n,o}} c_{j_1,\hat{s}_n,\alpha}^\dagger c_{j_2,\hat{s}_o,\gamma} (1 - \hat{n}_{j,\hat{s}_m,\beta}) + S^b S^a \sigma_{\beta\gamma}^b \sigma_{\alpha\beta}^a \sum_{\substack{(j_1,j_2 < j), \\ n,o}} c_{j_2,\hat{s}_o,\gamma} c_{j_1,\hat{s}_n,\alpha}^\dagger \hat{n}_{j,\hat{s}_m,\beta} \right] \\
& + \sum_{\substack{m=1, \\ \beta=\uparrow/\downarrow}}^{n_j} \frac{(J^{(j)})^2}{2(2\omega\tau_{j,\hat{s}_m,\beta} - \epsilon_{j,l}\tau_{j,\hat{s}_m,\beta} - J^{(j)}S^z s_{j,\hat{s}_m}^z)} \left[ S^x S^y \sigma_{\alpha\beta}^x \sigma_{\beta\alpha}^y c_{j,\hat{s}_m,\alpha}^\dagger c_{j,\hat{s}_m,\beta} c_{j,\hat{s}_m,\beta}^\dagger c_{j,\hat{s}_m,\alpha} \right. \\
& \left. + S^y S^x \sigma_{\alpha\beta}^x \sigma_{\beta\alpha}^y c_{j,\hat{s}_m,\beta}^\dagger c_{j,\hat{s}_m,\alpha} c_{j,\hat{s}_m,\alpha}^\dagger c_{j,\hat{s}_m,\beta} \right]. \tag{62}
\end{aligned}$$

The first term in eq.(62) corresponds to the renormalization of the Kondo coupling and describes the s-d exchange interactions for the entangled degrees of freedom

$$\begin{aligned}
\Delta H_{(j)}^1 = & \sum_{\substack{m=1, \\ \beta=\uparrow/\downarrow}}^{n_j} \frac{(J^{(j)})^2 \tau_{j,\hat{s}_m,\beta}}{(2\omega\tau_{j,\hat{s}_m,\beta} - \epsilon_{j,l}\tau_{j,\hat{s}_m,\beta} - J^{(j)}S^z s_{j,\hat{s}_m}^z)} \sum_{\substack{(j_1,j_2 < j), \\ n,o}} \mathbf{S} \cdot c_{j_1,\hat{s}_n,\alpha}^\dagger \frac{\sigma_{\alpha\beta}}{2} c_{j_2,\hat{s}_o,\beta} \\
= & \frac{1}{2} \sum_{\substack{m=1, \\ \beta=\uparrow/\downarrow}}^{n_j} \frac{\tau_{j,\hat{s}_m,\beta} (J^{(j)})^2 [(2\omega\tau_{j,\hat{s}_m,\beta} - \epsilon_{j,l}\tau_{j,\hat{s}_m,\beta}) + J^{(j)}S^z s_{j,m}^z]}{(\omega - \frac{\epsilon_{j,l}}{2})^2 - \frac{(J^{(j)})^2}{16}} \sum_{\substack{(j_1,j_2 < j), \\ n,o}} \mathbf{S} \cdot c_{j_1,\hat{s}_n,\alpha}^\dagger \frac{\sigma_{\alpha\beta}}{2} c_{j_2,\hat{s}_o,\beta} \\
= & \frac{1}{2} \sum_{\substack{m=1, \\ \beta=\uparrow/\downarrow}}^{n_j} \frac{(J^{(j)})^2 [(\frac{\omega}{2} - \frac{\epsilon_{j,l}}{4})]}{(\omega - \frac{\epsilon_{j,l}}{2})^2 - \frac{(J^{(j)})^2}{16}} \sum_{\substack{(j_1,j_2 < j), \\ n,o}} \mathbf{S} \cdot c_{j_1,\hat{s}_n,\alpha}^\dagger \frac{\sigma_{\alpha\beta}}{2} c_{j_2,\hat{s}_o,\beta} \\
& + \frac{1}{2} \sum_{m=1}^{n_j} \frac{(J^{(j)})^3 S^z s_{j,m}^z (\tau_{j,\hat{s}_m,\uparrow} + \tau_{j,\hat{s}_m,\downarrow})}{(\omega - \frac{\epsilon_{j,l}}{2})^2 - \frac{(J^{(j)})^2}{16}} \sum_{\substack{(j_1,j_2 < j), \\ n,o}} \mathbf{S} \cdot c_{j_1,\hat{s}_n,\alpha}^\dagger \frac{\sigma_{\alpha\beta}}{2} c_{j_2,\hat{s}_o,\beta} \tag{63}
\end{aligned}$$

$$\begin{aligned}
= & \frac{n_j (J^{(j)})^2 [(\omega - \frac{\epsilon_{j,l}}{2})]}{(\omega - \frac{\epsilon_{j,l}}{2})^2 - \frac{(J^{(j)})^2}{16}} \mathbf{S} \cdot \sum_{\substack{(j_1,j_2 < j), \\ n,o}} c_{j_1,\hat{s}_n,\alpha}^\dagger \frac{\sigma_{\alpha\gamma}}{2} c_{j_2,\hat{s}_o,\gamma}. \tag{64}
\end{aligned}$$

In the second last step of the calculation (eq.(63)), we have used the result  $\tau_{j,\hat{s}_m,\uparrow}^2 = \frac{1}{4}$ , where  $\tau_{j,\hat{s}_m,\uparrow} = \hat{n}_{j,\hat{s}_m,\uparrow} - \frac{1}{2}$ . In obtaining the last step of the calculation we have assumed  $\epsilon_{j,l} = \epsilon_j$  for a circular Fermi surface geometry. Further, we have replaced  $\tau_{j,\hat{s}_m,\uparrow}$  and  $\tau_{j,\hat{s}_m,\downarrow}$  by their eigenvalues,  $\tau_{j,\hat{s}_m,\uparrow} = -\tau_{j,\hat{s}_m,\downarrow} = \frac{1}{2}$ , i.e., the resulting decoupled electronic wave vector  $|j, \hat{s}_m\rangle$  carries a non-zero spin angular momentum. This configuration promotes the spin scattering between the Kondo impurity and the fermionic bath.

The second term in eq.(62) corresponds to the renormalization of the number diagonal Hamiltonian for the immediately disentangled electronic states  $|j, \hat{s}_m, \sigma\rangle$

$$\begin{aligned}
\Delta H_{(j)}^2 &= \sum_{\substack{m=1, \\ \beta=\uparrow/\downarrow}}^{n_j} \frac{(J^{(j)})^2}{(2\omega\tau_{j,\hat{s}_m,\beta} - \epsilon_{j,l}\tau_{j,\hat{s}_m,\beta} - J^{(j)}S^z s_{j,\hat{s}_m}^z)} \left[ S^x S^y \sigma_{\alpha\beta}^x \sigma_{\beta\alpha}^y c_{j,\hat{s}_m,\alpha}^\dagger c_{j,\hat{s}_m,\beta} c_{j,\hat{s}_m,\beta}^\dagger c_{j,\hat{s}_m,\alpha} \right. \\
&\quad \left. + S^y S^x \sigma_{\alpha\beta}^x \sigma_{\beta\alpha}^y c_{j,\hat{s}_m,\beta}^\dagger c_{j,\hat{s}_m,\alpha} c_{j,\hat{s}_m,\alpha}^\dagger c_{j,\hat{s}_m,\beta} \right] \\
&= \sum_{\substack{m=1, \\ \beta=\uparrow/\downarrow}}^{n_j} \frac{(J^{(j)})^2}{(2\omega\tau_{j,\hat{s}_m,\beta} - \epsilon_{j,l}\tau_{j,\hat{s}_m,\beta} - J^{(j)}S^z s_{j,\hat{s}_m}^z)} S^z \frac{\sigma_{\alpha\alpha}^z}{2} \left[ \hat{n}_{j,\hat{s}_m,\alpha}(1 - \hat{n}_{j,\hat{s}_m,\beta}) - \hat{n}_{j,\hat{s}_m,\beta}(1 - \hat{n}_{j,\hat{s}_m,\alpha}) \right] \\
&= \sum_{m=1}^{n_j} \frac{(J^{(j)})^2}{(2\omega\tau_{j,\hat{s}_m,\beta} - \epsilon_{j,l}\tau_{j,\hat{s}_m,\beta} - J^{(j)}S^z s_{j,\hat{s}_m}^z)} S^z s_{j,\hat{s}_m}^z, \tag{65}
\end{aligned}$$

where we have used  $\hat{n}_{j,\hat{s}_m,\alpha}(1 - \hat{n}_{j,\hat{s}_m,\beta}) - \hat{n}_{j,\hat{s}_m,\beta}(1 - \hat{n}_{j,\hat{s}_m,\alpha}) = \hat{n}_{j,\hat{s}_m,\alpha} - \hat{n}_{j,\hat{s}_m,\beta}$  in the last step, and the spin density for the state  $|j, \hat{s}_m\rangle$  is given by  $s_{j,\hat{s}_m}^z = \frac{1}{2}(\hat{n}_{j,\hat{s}_m,\uparrow} - \hat{n}_{j,\hat{s}_m,\downarrow})$ .

In obtaining the above RG equation we have replaced  $\hat{\omega}_{(j)} = 2\omega\tau_{j,\hat{s}_m,\beta}$ . We set the electronic configuration  $\tau_{j,\hat{s}_m,\uparrow} = -\tau_{j,\hat{s}_m,\downarrow} = \frac{1}{2}$  to account for the spin scattering between the Kondo impurity and the fermionic bath. The operator  $\hat{\omega}_{(j)}$  (eq.(7)) for RG step  $j$  is determined by the occupation number diagonal piece of the Hamiltonian  $H_{(j-1)}^D$  attained at the next RG step  $j - 1$ . This demands a self-consistent treatment of the RG equation to determine the  $\omega$ . In this fashion, two-particle and higher order quantum fluctuations are automatically encoded into the RG dynamics of  $\hat{\omega}$ . In the present work, however, we restrict our study by ignoring the RG contribution in  $\omega$ . The electron/hole configuration ( $|1_{j,\hat{s}_m,\beta}\rangle/|0_{j,\hat{s}_m,\beta}\rangle$ ) of the disentangled electronic state (and associated with energy  $\pm\epsilon_{j,l}$ ) is accounted by the fluctuation energy scales  $\pm\omega$ .

From the above Hamiltonian RG equations eq.(64), we can obtain the form of the Kondo coupling RG equation

$$\Delta J^{(j)} = \frac{n_j (J^{(j)})^2 \left[ \omega - \frac{\epsilon_{j,l}}{2} \right]}{\left( \frac{\epsilon_{j,l}}{2} - \omega \right)^2 - \frac{(J^{(j)})^2}{16}}. \tag{66}$$

- 
- [1] J. Kondo, Resistance minimum in dilute magnetic alloys, Progress of theoretical physics **32**, 37 (1964).
- [2] P. W. Anderson and G. Yuval, Exact results in the kondo problem: equivalence to a classical one-dimensional coulomb gas, Physical Review Letters **23**, 89 (1969).

- [3] P. W. Anderson, G. Yuval, and D. Hamann, Exact results in the kondo problem. ii. scaling theory, qualitatively correct solution, and some new results on one-dimensional classical statistical models, *Physical Review B* **1**, 4464 (1970).
- [4] P. Anderson, A poor man’s derivation of scaling laws for the kondo problem, *Journal of Physics C: Solid State Physics* **3**, 2436 (1970).
- [5] N. Andrei, K. Furuya, and J. H. Lowenstein, Solution of the kondo problem, *Rev. Mod. Phys.* **55**, 331 (1983).
- [6] A. M. Tsvelick and P. B. Wiegmann, Exact results in the theory of magnetic alloys, *Adv. in Phys.* **32**, 453 (1983).
- [7] K. G. Wilson, The renormalization group: Critical phenomena and the kondo problem, *Rev. Mod. Phys.* **47**, 773 (1975).
- [8] R. Bulla, T. Costi, and T. Pruschke, Numerical renormalisation group method for quantum impurity systems, *Rev. Mod. Phys.* **80**, 395 (2008).
- [9] I. Affleck, Conformal field theory approach to the kondo effect, arXiv preprint cond-mat/9512099 (1995).
- [10] I. Affleck and A. W. Ludwig, Exact conformal-field-theory results on the multichannel kondo effect: Single-fermion greens function, self-energy, and resistivity, *Physical Review B* **48**, 7297 (1993).
- [11] P. Nozieres, A “fermi-liquid” description of the kondo problem at low temperatures, *Journal of Low Temperature Physics* **17**, 31 (1974).
- [12] M. Nozaki, S. Ryu, and T. Takayanagi, Holographic geometry of entanglement renormalization in quantum field theories, *Journal of High Energy Physics* **2012**, 193 (2012).
- [13] G. Yoo, S.-S. Lee, and H.-S. Sim, Detecting kondo entanglement by electron conductance, *Physical review letters* **120**, 146801 (2018).
- [14] A. Mukherjee and S. Lal, Scaling theory for mott-hubbard transitions-i:  $T=0$  phase diagram of the  $1/2$ -filled hubbard model, arxiv preprint arxiv:2004.06900 (2019).
- [15] a. A. Mukherjee and S. Lal, Unitary renormalisation group for correlated electrons-i: a tensor network approach, arXiv preprint arXiv:2004.06897 (2020).
- [16] P. Coleman, *Introduction to many-body physics* (Cambridge University Press, 2015) chapter:18.
- [17] R. M. Martin, Fermi-surface sum rule and its consequences for periodic kondo and mixed-

- valence systems, Physical Review Letters **48**, 362 (1982).
- [18] B. Groisman, S. Popescu, and A. Winter, Quantum, classical, and total amount of correlations in a quantum state, Phys. Rev. A **72**, 032317 (2005).